ACS Energy LETTERS

http://pubs.acs.org/journal/aelccp

LETTER

Monolithic Two-Terminal Perovskite/Perovskite/Silicon Triple-Junction Solar Cells with Open Circuit Voltage >2.8 V

Maryamsadat Heydarian,* Minasadat Heydarian, Alexander J. Bett, Martin Bivour, Florian Schindler, Martin Hermle, Martin C. Schubert, Patricia S. C. Schulze, Juliane Borchert, and Stefan W. Glunz

Cite This: *ACS Energy Lett.* 2023, 8, 4186−4192

Read Online

ACCESS | Metrics & More | Article Recommendations | Supporting Information

ABSTRACT: **The efficiency of perovskite/silicon tandem solar cells has exceeded the previous record for III−V-based dual-junction solar cells. This shows the high potential of perovskite solar cells in multi-junction applications. Perovskite/perovskite/silicon triple-junction solar cells are now the next step to achieve efficient and low-cost multi-junction solar cells with an efficiency potential even higher than that for dual-junction solar cells. Here we present a perovskite/perovskite/silicon triple-junction solar cell with an open circuit voltage of >2.8 V, which is the record value reported for this structure so far. This is achieved through employing a gas quenching method for deposition of the top perovskite layer as well as optimization of interlayers between perovskite subcells. Moreover, for the measurement of our triple-junction solar cells, precise measurement procedures are implemented to ensure the reliability and accuracy of the reported values.**

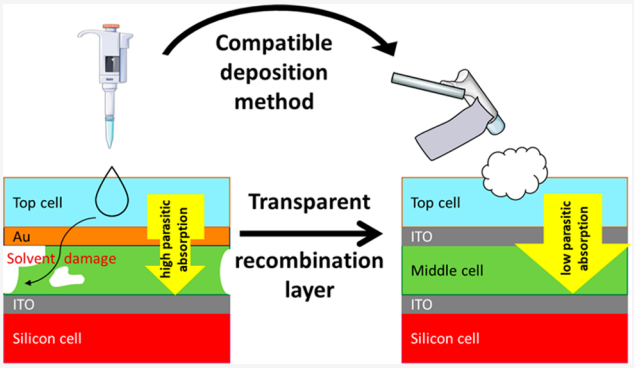

The worldwide installed capacity of photovoltaics (PVs) has now reached its 1 TW_{dc} milestone.[1] With entering the terawatt scale, rapid actions to reduce the cost of PV technology is more important than ever, which is possible by increasing the efficiency of the PV modules.[1] The most common and promising approach to overcome the efficiency limit of single-junction silicon solar cells is to couple them with high bandgap (HBG) solar cells in a multi-junction structure. Over recent years, metal halide perovskites have proven to be an excellent material class with potentially low process costs for multi-junction applications. The record efficiency of 33.7% for perovskite/silicon tandem solar cells is now the highest efficiency reported for a dual-junction structure.[2] It is possible to further increase the efficiency by adding to the number of junctions.[3] Currently, triple-junction solar cells based on III−V semiconductor materials, with a power conversion efficiency of 39.5%, are the most efficient multi-junction solar cells under the Air Mass 1.5 global (AM1.5g) spectrum, even higher than the previous sextuple-junction solar cell record,[4] but the high cost of the III−V solar cells makes them unsuitable for terrestrial application. Hence, perovskite/perovskite/silicon triple-junction solar cells are the next focus of the perovskite community. However, this technology is relatively new, and the research on it is at an early stage with only a few demonstrations.[5−7] Among the possible approaches to couple the subcells in multi-junction solar cells, the two-terminal architecture is likely to be the most relevant for the future market, as it can easily be integrated into the standard module layout of silicon technology and requires fewer interconnections. In monolithic two-terminal multi-junction solar cells, the subcells are connected in series. Therefore, the current is limited by the subcell that has the lowest current and the voltage of the final device is the sum of the voltages of individual subcells. In that respect, high open circuit voltage is a key milestone that needs to be achieved to construct a highly efficient two-terminal multi-junction solar cell. To ensure the highest voltage, it is crucial to maximize the voltage of individual subcells and to minimize the voltage losses at the interconnections of the subcells. The latter is not trivial for monolithically integrated triple-junction solar cells, as they

Received: July 10, 2023
Accepted: August 21, 2023
Published: September 15, 2023

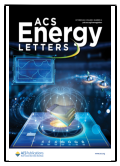

https://doi.org/10.1021/acsenergylett.3c01391
ACS Energy Lett. 2023, 8, 4186−4192

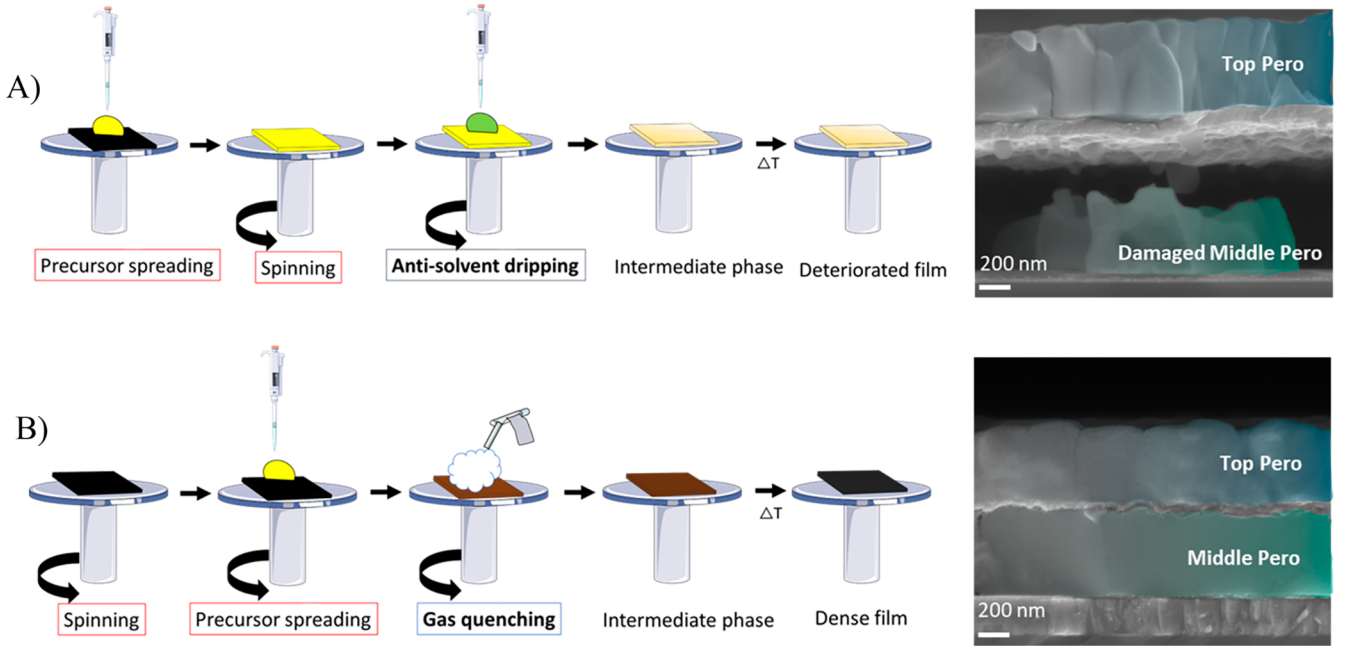

Figure 1. Schematic of the wet-chemical deposition steps and SEM cross section images of the middle perovskite cell/top perovskite stack using (A) the standard antisolvent deposition route and (B) an adapted gas quenching technique. Using the adapted gas quenching technique allows the formation of the perovskite top absorber on the perovskite middle cell without damaging the film.

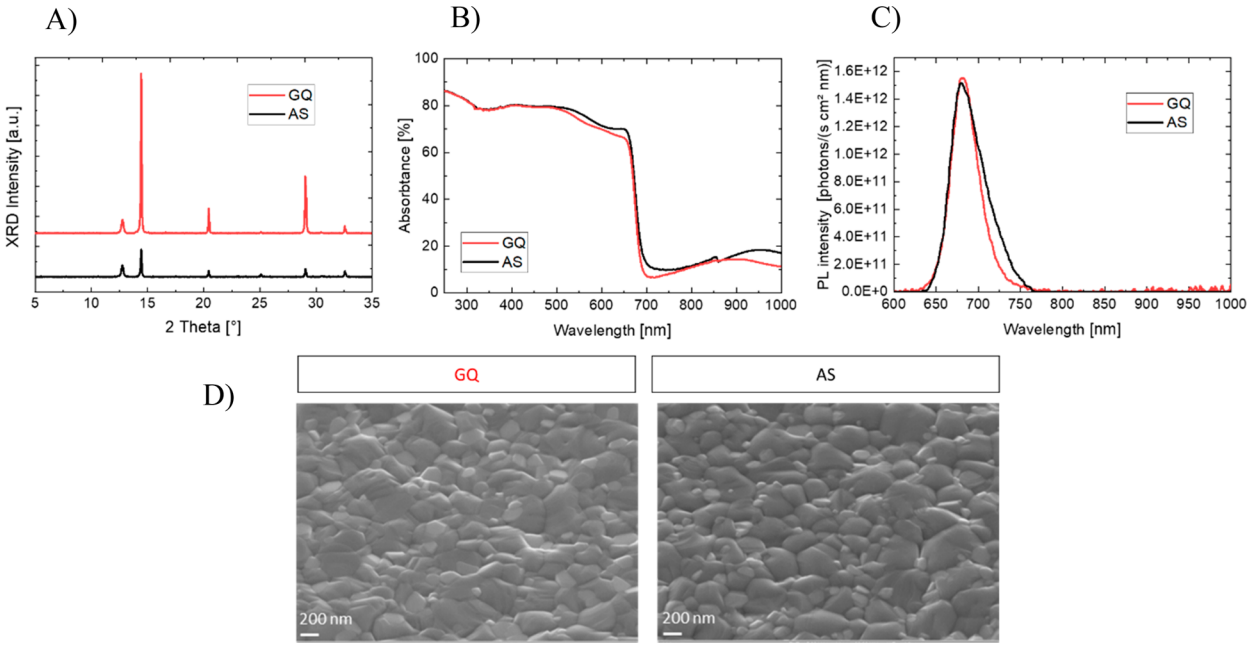

Figure 2. Comparison of (A) XRD patterns, (B) absorptance spectra, (C) PL spectra, and (D) top-view SEM images of the HBG perovskite films prepared with standard antisolvent and adapted gas quenching methods. Film formation and quality for the perovskites deposited with two methods are comparable.

consist of multiple layers processed sequentially on top of each other and the addition of each single layer introduces new challenges in terms of compatibility and interaction with other layers. In this regard, a major challenge associated with perovskite/perovskite/silicon triple-junction solar cells is the process compatibility with the underlying layers. Especially the solvent involved in the processing of the top perovskite layer can be harmful to the middle perovskite subcell, since both perovskites share similar solvent systems. The second challenge is developing a lossless interconnection layer between the perovskite subcells. In this work, we employ a damage-free deposition method for processing of the perovskite top cell and optimize the interconnection layers between perovskite middle and top cells. Combining these two optimizations, we present a monolithic two-terminal perovskite/perovskite/silicon triple-junction solar cell processed on a flat front and rear textured silicon hetero-junction (SHJ) bottom cell. Our best device shows an open circuit voltage (V_{OC}) of 2.86 V, which is higher than previously reported values for perovskite/perovskite/silicon triple-junction solar cells, a fill factor (*FF*) of 78%, a

https://doi.org/10.1021/acsenergylett.3c01391
ACS Energy Lett. 2023, 8, 4186−4192

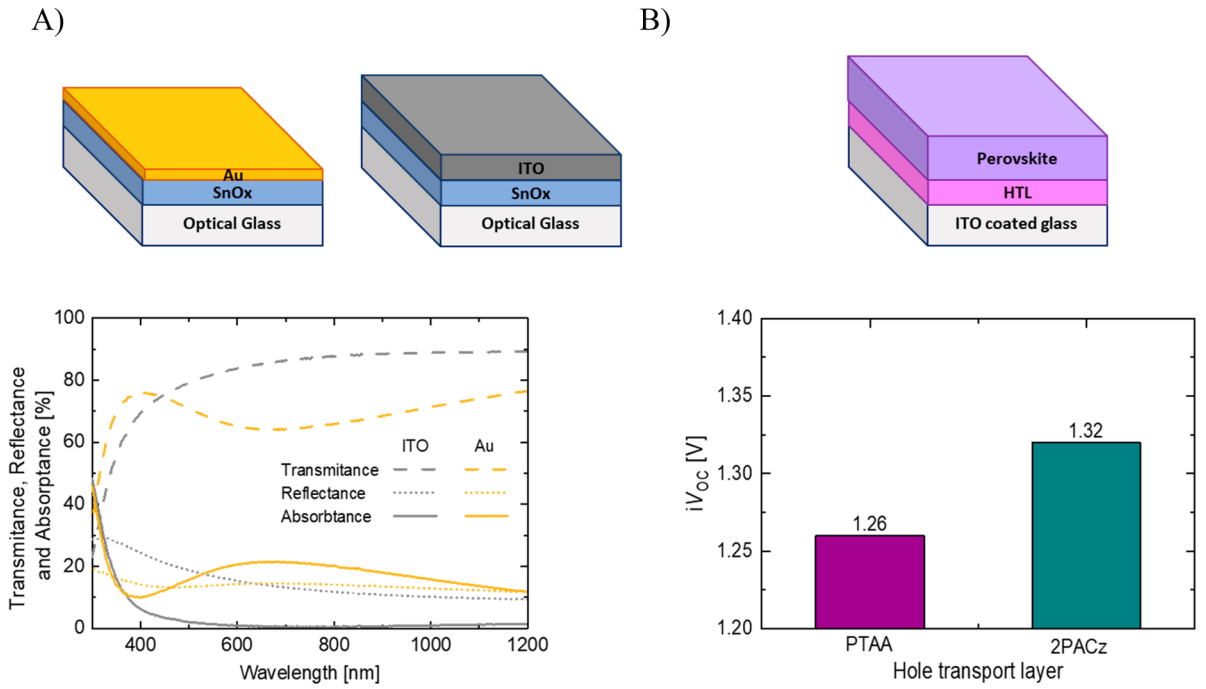

Figure 3. (A) Transmittance, reflectance, and absorptance spectra of 15 nm ITO and 1 nm Au deposited on an optical glass/SnO_x stack. (B) iV_{OC} values for HBG perovskite on PTAA and 2PACz HTL derived from absolute PL measurements. ITO shows better transparency and less parasitic absorption compared to the Au layer. Perovskite processed on 2PACz shows a higher iV_{OC} compared to perovskite with PTAA as HTL.

short-circuit current density (j_{SC}) of 8.9 mA/cm^2, and a power conversion efficiency (*PCE*) of 20.0%.

The middle perovskite absorber in our structure is a triple cation perovskite with $Cs_{0.05}(FA_{0.9}MA_{0.1})_{0.95}Pb(I_{0.95}Br_{0.05})_3$ composition exhibiting a bandgap of 1.56 eV while the top perovskite absorber is a $Cs_{0.05}(FA_{0.55}MA_{0.45})_{0.95}Pb(I_{0.55}Br_{0.45})_3$ perovskite with a 1.83 eV bandgap determined from Tauc plot (Figure S2). We note that the bandgaps combined in this work are not the final optimum bandgaps for a triple-junction solar cell.[3] However, the focus of this paper is on process optimization and integration of the subcells into triple-junction devices, and the findings are applicable to other perovskite compositions.

One of the main challenges for solution-based processing of absorbers in multi-junction solar cells is the possible solvent damage to the underlying layers. The most widely used method for fabrication of perovskite layers using spin coating is the antisolvent (AS) method, in which a solution of the perovskite precursors is spread on the substrate prior to spin coating. Then, an adequate amount of antisolvent, e.g., ethyl acetate or chlorobenzene, is dripped on the spinning sample to trigger the crystallization process, followed by an annealing step. However, since both perovskite absorbers have the same solvent system, during the processing of the top perovskite, the solvents involved in the process can dissolve the perovskite underneath. We clearly observe this effect in cross-sectional scanning electron microscopy (SEM) images (Figure 1A), where the middle perovskite is damaged by the solvent during processing of the perovskite top layer. To overcome this issue, we adapted the deposition of the top perovskite layer. For this purpose, standard static spin coating is replaced by dynamic spin coating, which minimizes the time that the solution is resting on the sample and prevents the dissolution of the underlying middle perovskite layer. Moreover, instead of using an antisolvent, a nitrogen flow is employed to extract the solvent from the precursor during the spin coating similar to the approach developed for single-junction perovskite solar cells in 2014 by Huang et al.[8] and used in several other works.[9−14] As a result of these adaptations, we were able to deposit a homogeneous black perovskite layer on top of the underlying perovskite cell (Figure 1B). The process optimization of the perovskite top layer is shown in Figure 1.

To compare the crystallinity of the high bandgap perovskite, X-ray diffraction (XRD) measurements were performed on the films deposited with these two techniques. XRD patterns of both films display similar peak positions (Figure 2A). In addition, the film prepared with the gas quenching (GQ) method shows higher diffraction peaks of perovskite at 14.4°, 20.4°, and 29°, indicating enhanced crystallinity. The PbI_2 peak at 12.8° arises from the 10% lead excess in the perovskite solution and is similar in both cases, which shows that the reaction has been completed despite the rapid crystallization when using GQ. The morphology of the perovskite films deposited with GQ and AS are compared and presented in Figure 2D. The top-view SEM images show no detrimental effect for the film deposited with the adapted technique, and both films show high-quality, compact and homogeneous perovskite layers with very similar grain sizes (Figure S3). The absorptance curves determined from the reflection and transmission measurements confirm a similar absorption in both perovskite layers (Figure 2B). In addition, photoluminescence (PL) spectra of both samples show a peak at 680 nm, corresponding to 1.82 eV (Figure 2C). The sample processed with GQ shows a stable PL peak position after 5 minutes of continuous illumination, which proves the photostability of the HBG perovskite despite the high amount of Br in the composition (Figure S4). Thus, by replacing the AS with the GQ method, we were able to form the top perovskite

https://doi.org/10.1021/acsenergylett.3c01391
ACS Energy Lett. 2023, 8, 4186−4192

absorber on top of the middle perovskite solar cell. In addition, the GQ approach has several other advantages such as elimination of additional solvents and compatibility with large-area deposition techniques.[9,13]

Another important feature of monolithic triple-junction solar cells is the recombination layer between the subcells. Since the subcells are connected in series through the recombination layer, it is crucial that this additional layer introduces minimum voltage losses and parasitic absorption. In general, there are two common approaches for connecting two perovskite subcells. The first approach is employing an evaporated ultrathin metal layer such as gold (Au), which is very common in all-perovskite[11,15−17] and organic tandem solar cells,[18] and the second approach is to employ a sputtered transparent conductive oxide (TCO) such as indium tin oxide (ITO) often used in perovskite/silicon tandem solar cells.[19−21] Even though many highly efficient all-perovskite solar cells have used 1 nm evaporated Au as the recombination layer,[11,15−17] recently thin TCO in the range of 5−15 nm was shown to be favorable in both all-perovskite[22] and perovskite/organic tandem solar cells.[23] In this work, we compared 1 nm of evaporated Au and 15 nm sputtered ITO as the recombination layers between the perovskite subcells in perovskite/perovskite/silicon triple-junction solar cells. To analyze the optical properties of these two layers, reflection and transmission measurements were performed on 15 nm ITO and 1 nm Au deposited on an optical glass/SnO_x stack (Figure 3A). We found that the ITO layers feature a better transparency and lower parasitic absorption compared to Au, as was reported previously.[22] The Au layer shows around 20% parasitic absorption in the wavelength range of 400−1200 nm, which limits the transmitted light from the top cells to the underlying subcells. Another disadvantage of employing Au as the recombination layer is that the common self-assembled monolayer (SAM) hole transport materials cannot be directly formed on it, as its anchoring group phosphonic acid requires hydroxyl groups to bind in a condensation reaction.[24] Therefore, in the case of the Au recombination layer, we employed poly[bis(4-phenyl)-(2,4,6-trimethylphenyl)amine] (PTAA) as the hole transport layer (HTL) of the top cell. However, it has previously been shown that especially for HBG perovskite, replacing PTAA with SAM as the HTL is necessary to minimize the interfacial nonradiative recombination at the HTL/perovskite interface and improve the V_{OC}.[19,21,25] Figure S5 compares the absolute PL measurements of the glass/HTL/perovskite stacks with PTAA and 2PACz SAM. The PL signal of the HBG perovskite on 2PACz is higher than on PTAA by 1 order of magnitude. Consequently, there is more than a 50 mV gain in the iV_{OC} value upon replacing PTAA with 2PACz (Figure 3B). Therefore, employment of ITO as a recombination layer not only is optically advantageous but also allows the integration of SAM as the HTL of HBG perovskite in our triple-junction solar cell structure.

To investigate the impact of these optimizations (Au/PTAA versus ITO/2PACz interconnections) on the performance of the devices, perovskite/perovskite/silicon triple-junction solar cells with the following architectures were developed: SHJ/ITO/PTAA/PFN/perovskite/C_{60}/SnO_x/**Au**/**PTAA**/PFN/perovskite/C_{60}/SnO_x/ITO/Ag/MgF_2, and SHJ/ITO/PTAA/PFN/perovskite/C_{60}/SnO_x/**ITO**/**2PACz**/perovskite/C_{60}/SnO_x/ITO/Ag/MgF_2 as shown in Figure 4A. The external quantum efficiency (EQE) measurements of the triple-junction devices are presented in Figure 4B. To measure the EQE of each subcell, the triple-junction solar cell was illuminated with spectrally selective bias LEDs (Figure S1) and an external bias voltage was applied to bring the subcell under measurement to short circuit condition according to refs 26 and 27. More details can be found in the Supporting Information. Even though the EQEs are not absolutely calibrated, considering the nonoptimized bandgaps used for the perovskite subcells, it is clear that the overall currents of the devices are limited by the middle cell.

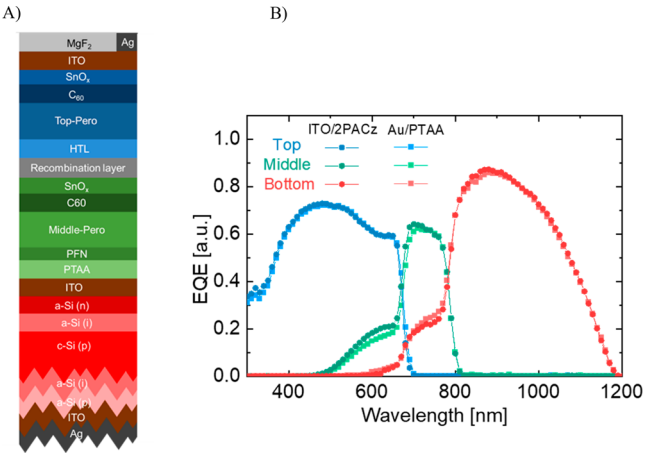

Figure 4. (A) Schematic of the perovskite/perovskite/silicon triple-junction device structure. (B) EQE curves of triple-junction solar cells with Au/PTAA and ITO/2PACz interconnection layers.

By replacing Au/PTAA with ITO/2PACz, more light is transmitted to the middle cell (Figure 3A) due to less parasitic absorption, and therefore, a higher j_{SC} is expected in the final triple-junction solar cell.

Finally, when measuring the current density−voltage (j−V) curve of a multi-junction solar cell, it is important to consider that the spectra of solar simulators do not perfectly match that of the Air Mass 1.5 global (AM1.5g) spectrum. Therefore, the solar simulator spectrum needs to be adjusted prior to the measurements in a way that all three subcells generate the same current under the simulator as they would under the AM1.5g spectrum. To perform this adjustment based on the spectral responses of the three subcells, a solar simulator with at least 3 different spectral channels is required.[28] Although such measurement procedure is very well established[28,29] and is also common for measurement of perovskite/silicon tandem solar cells, so far it has not been employed for measurements of perovskite-based triple-junction solar cells. Here, we report the j−V curves of perovskite/perovskite/silicon triple-junction solar cells measured under a spectrum-adjusted solar simulator. We performed the j−V measurement with a light-emitting diode (LED) based solar simulator equipped with 20 spectrally independent LEDs. The spectrum is adjusted using the algorithm developed in ref 30 to ensure that the following requirements are fulfilled:

$$j_{\text{top}}^{\text{simulator}} = j_{\text{top}}^{\text{AM1.5g}}$$

$$j_{\text{middle}}^{\text{simulator}} = j_{\text{middle}}^{\text{AM1.5g}}$$

$$j_{\text{bottom}}^{\text{simulator}} = j_{\text{bottom}}^{\text{AM1.5g}}$$

We note that only relative spectral responses are needed for this procedure.[28] Best-performing j−V curves of both groups

https://doi.org/10.1021/acsenergylett.3c01391
ACS Energy Lett. 2023, 8, 4186−4192

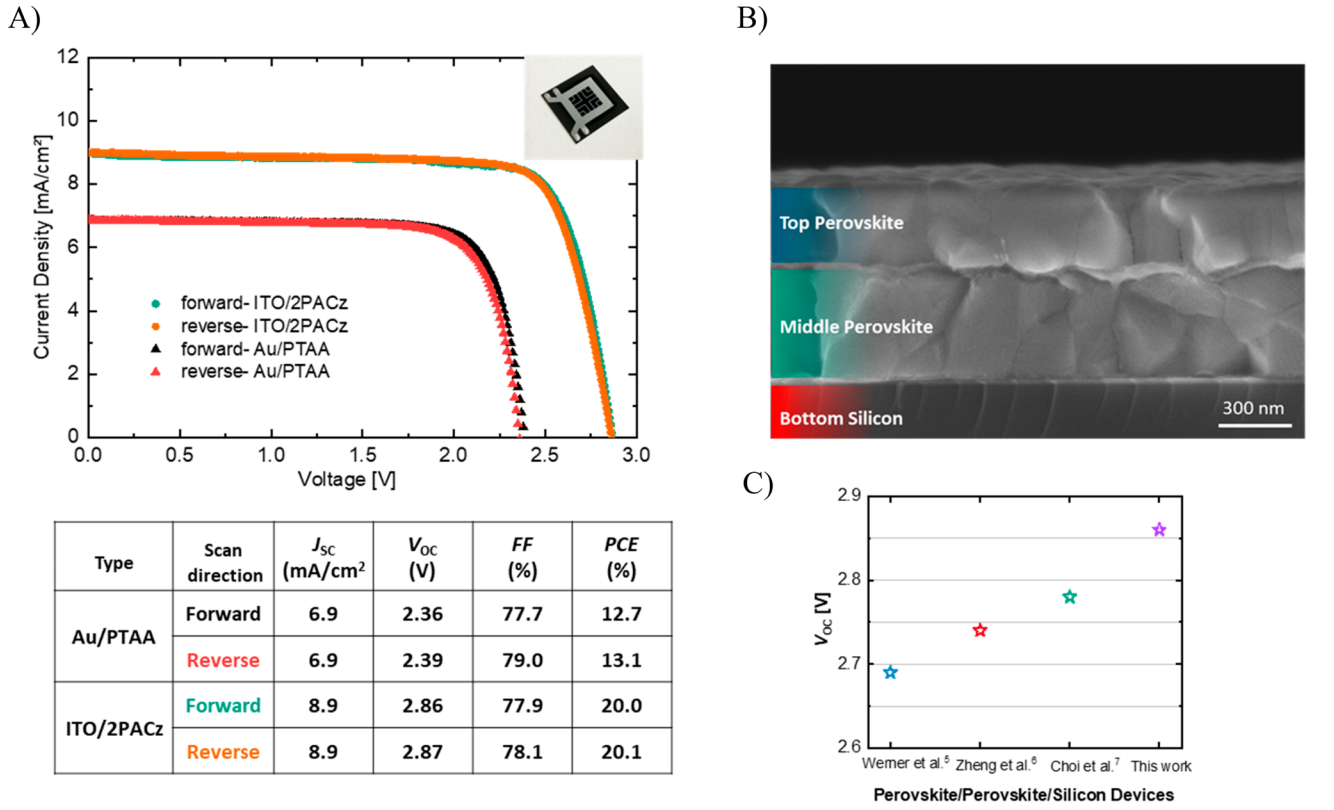

Type	Scan direction	J_{SC} (mA/cm²)	V_{OC} (V)	*FF* (%)	*PCE* (%)
Au/PTAA	Forward	6.9	2.36	77.7	12.7
	Reverse	6.9	2.39	79.0	13.1
ITO/2PACz	Forward	8.9	2.86	77.9	20.0
	Reverse	8.9	2.87	78.1	20.1

Figure 5. (A) Exemplary photograph of a triple-junction solar cell, best-performing *j*−*V* curves, and photovoltaic parameters of perovskite/perovskite/silicon devices with Au/PTAA and ITO/2PACz interconnection layers. (B) SEM cross section image of the silicon/ITO/PTAA/middle perovskite/C_{60}/SnO_x/ITO/2PACz/top perovskite and (C) evolution of the V_{OC} in reported Perovskite/Perovskite/Silicon publications. The V_{OC} achieved in this work is a further improvement with V_{OC} > 2.8 V.

are presented in Figure 5. Samples with ITO/2PACz interconnection layers exhibit increased j_{SC} as well as V_{OC}, as expected from the optical advantage of the ITO compared to Au (which increases the current of the middle cell) and reduced nonradiative recombination at the perovskite/2PACz interface compared to perovskite/PTAA (which increases the V_{OC} of the top cell).

The best-performing cell shows 20.0% *PCE*, a *FF* of 78%, and a j_{SC} of 8.9 mA/cm^2. The *PCE* evolution over 6 minutes at a fixed voltage close to the maximum power point voltage is shown in Figure S6. Our device shows a V_{OC} of more than 2.8 V, which is higher than the previously reported V_{OC} for perovskite/perovskite/silicon triple-junction solar cells (Figure 5C) even though the HBG perovskite in this work has a bandgap of 1.83 eV, which is lower than the 1.90 and 1.96 eV perovskites employed in refs 6 and 7. Under 1 sun illumination, the open circuit voltages of our top and middle perovskites in single-junction solar cells are ∼1.12 and ∼1.02 V, respectively (Figure S7). The SHJ bottom cell in this work has a V_{OC} of ∼0.73 V. Therefore, there is negligible voltage loss in the final triple-junction devices, which shows the high quality of the recombination layers between the subcells. We note that higher V_{OC} values have been reported for triple-junction solar cells using a perovskite or organic bottom cell.[31,32] However, a voltage difference is expected between the technologies, as the silicon solar cell has a lower voltage compared to the other two bottom cells with bandgaps of 1.2 and 1.3 eV for perovskite and organic solar cells, respectively.[31,32]

On a final note, we noticed that even though the adapted processing minimizes the damage to the middle cell, in order to have better process reproducibility, it is crucial to improve the solvent barrier function of the interlayers. From the SEM top-view image (see Figure S8), island-like growth of the 1 nm Au on silicon is obvious, similar to what has been previously shown for 1 nm silver (Ag) layers.[23] This resulted in incomplete surface coverage, while the 15 nm ITO features a homogeneous close layer (Figure S8), making ITO a better solvent barrier. However, since in our work the ITO layer is sputtered through a shadow mask with a 1 cm^2 opening, it was not protective enough against the solvent penetration. Therefore, as a next step, we investigated the solvent barrier property of our SnO_x layer with different thicknesses. We observed that 20 nm SnO_x shows no resistance against the solvent and leads to fast penetration of the solvent to the underlying layers. Increasing the thickness of SnO_x to 30 and 40 nm resulted in a better solvent resistivity and therefore can protect the underlying layers more effectively (Figure S9). Moreover, the absorptance curves of the SnO_x layer with different thicknesses exhibit no additional parasitic absorption for the thicker SnO_x layer (Figure S10). The triple-junction solar cells with 30 nm thick SnO_x in combination with the ITO recombination layer resulted in an improved yield and showed little spread in the data (Figure S11).

In summary, this paper addresses some key challenges for the development and characterization of monolithic two-terminal perovskite/perovskite/silicon triple-junction solar cells. For the first time, a gas quenching method is employed for the processing of the perovskite top cell in a triple-junction

https://doi.org/10.1021/acsenergylett.3c01391
ACS Energy Lett. 2023, 8, 4186−4192

structure, which allows for homogeneous formation of the HBG perovskite absorber and prevents solvent damage to the underlying layers. Furthermore, the ITO/2PACz interconnection layers between the perovskite subcells show almost no voltage loss. The main limiting factor of our device comes from the low short-circuit current density, which is limited by the current of the middle cell. This could be overcome by adaptation of the bandgaps and thicknesses of the perovskite subcells. In addition, even though the voltage achieved here is equal to the sum of the voltages of the individual subcells, it can further be increased by improving the voltage of the middle and top perovskite cells. Overall, perovskite-based triple-junction solar cells are a complex new technology. Our work points out some encouraging solutions for robust processing of highly efficient triple-junction cells with high voltages. Further optimizations are required to bring it to the level of perovskite/silicon dual-junction solar cells and eventually surpass them. Moreover, the long-term stability of these solar cells under standard test conditions and elevated temperature needs to be addressed in future work. Finally, for commercialization of perovskite-based multi-junction solar cells, an efficiency increase needs to be achieved using scalable techniques on industrial silicon wafers.

■ ASSOCIATED CONTENT

Supporting Information

The Supporting Information is available free of charge at https://pubs.acs.org/doi/10.1021/acsenergylett.3c01391.

Details on materials, solution preparation, solar cell fabrication, EQE measurements, $j-V$ measurements, PL measurements, SEM measurements, and XRD measurements, Tauc plot of the middle and top perovskites, apparent grain size of the top perovskite, PL spectra of top perovskite over time, PL spectra of top perovskite on different hole transport layers, efficiency of triple-junction solar cell over time, $j-V$ measurements of the single-junction solar cells, SEM images of the recombination layers, solvent resistance function of different interlayers, reflectance/transmittance/absorptance spectra of SnO_x layers with different thicknesses, and statistical photovoltaic parameters of triple-junction solar cells (PDF)

■ AUTHOR INFORMATION

Corresponding Author

Maryamsadat Heydarian − *Fraunhofer Institute for Solar Energy Systems, 79110 Freiburg, Germany;* orcid.org/0000-0002-4053-0888; Email: Maryamsadat.Heydarian@ise.fraunhofer.de

Authors

Minasadat Heydarian − *Fraunhofer Institute for Solar Energy Systems, 79110 Freiburg, Germany; University of Freiburg, Department of Sustainable Systems Engineering (INATECH), 79110 Freiburg, Germany*

Alexander J. Bett − *Fraunhofer Institute for Solar Energy Systems, 79110 Freiburg, Germany;* orcid.org/0000-0003-0312-6701

Martin Bivour − *Fraunhofer Institute for Solar Energy Systems, 79110 Freiburg, Germany*

Florian Schindler − *Fraunhofer Institute for Solar Energy Systems, 79110 Freiburg, Germany*

Martin Hermle − *Fraunhofer Institute for Solar Energy Systems, 79110 Freiburg, Germany*

Martin C. Schubert − *Fraunhofer Institute for Solar Energy Systems, 79110 Freiburg, Germany*

Patricia S. C. Schulze − *Fraunhofer Institute for Solar Energy Systems, 79110 Freiburg, Germany;* orcid.org/0000-0002-1924-6153

Juliane Borchert − *Fraunhofer Institute for Solar Energy Systems, 79110 Freiburg, Germany; University of Freiburg, Department of Sustainable Systems Engineering (INATECH), 79110 Freiburg, Germany*

Stefan W. Glunz − *Fraunhofer Institute for Solar Energy Systems, 79110 Freiburg, Germany; University of Freiburg, Department of Sustainable Systems Engineering (INATECH), 79110 Freiburg, Germany*

Complete contact information is available at: https://pubs.acs.org/10.1021/acsenergylett.3c01391

Notes

The authors declare no competing financial interest.

■ ACKNOWLEDGMENTS

This work was partially supported by the European Union through the Horizon Europe project Triumph under the number 101075725 and the German Federal Ministry for Economic Affairs and Climate Action (BMWK) under contract number 03EE1132A (RIESEN). The authors thank K. Fischer, J. Myers, F. Martin, and J. Zielonka for technical and measurement support.

■ REFERENCES

(1) Haegel, N. M.; Verlinden, P.; Victoria, M.; Altermatt, P.; Atwater, H.; Barnes, T.; Breyer, C.; Case, C.; de Wolf, S.; Deline, C.; Dharmrin, M.; Dimmler, B.; Gloeckler, M.; Goldschmidt, J. C.; Hallam, B.; Haussener, S.; Holder, B.; Jaeger, U.; Jaeger-Waldau, A.; Kaizuka, I.; Kikusato, H.; Kroposki, B.; Kurtz, S.; Matsubara, K.; Nowak, S.; Ogimoto, K.; Peter, C.; Peters, I. M.; Philipps, S.; Powalla, M.; Rau, U.; Reindl, T.; Roumpani, M.; Sakurai, K.; Schorn, C.; Schossig, P.; Schlatmann, R.; Sinton, R.; Slaoui, A.; Smith, B. L.; Schneidewind, P.; Stanbery, B. J.; Topič, M.; Tumas, W.; Vasi, J.; Vetter, M.; Weber, E.; Weeber, A. W.; Weidlich, A.; Weiss, D.; Bett, A. W. Photovoltaics at multi-terawatt scale: Waiting is not an option. *Science* **2023**, *380*, 39−42.

(2) Interactive Best Research-Cell Efficiency Chart, 2023. https://www.nrel.gov/pv/interactive-cell-efficiency.html (accessed 15 June 2023).

(3) Schygulla, P.; Müller, R.; Lackner, D.; Höhn, O.; Hauser, H.; Bläsi, B.; Predan, F.; Benick, J.; Hermle, M.; Glunz, S. W.; Dimroth, F. Two-terminal III−V//Si triple-junction solar cell with power conversion efficiency of 35.9% at AM1.5g. *Prog. Photovoltaics* **2022**, *30*, 869.

(4) France, R. M.; Geisz, J. F.; Song, T.; Olavarria, W.; Young, M.; Kibbler, A.; Steiner, M. A. Triple-junction solar cells with 39.5% terrestrial and 34.2% space efficiency enabled by thick quantum well superlattices. *Joule* **2022**, *6*, 1121−1135.

(5) Werner, J.; Sahli, F.; Fu, F.; Diaz Leon, J. J.; Walter, A.; Kamino, B. A.; Niesen, B.; Nicolay, S.; Jeangros, Q.; Ballif, C. Perovskite/Perovskite/Silicon Monolithic Triple-Junction Solar Cells with a Fully Textured Design. *ACS Energy Letters* **2018**, *3*, 2052−2058.

(6) Zheng, J.; Wang, G.; Duan, W.; Mahmud, M. A.; Yi, H.; Xu, C.; Lambertz, A.; Bremner, S.; Ding, K.; Huang, S.; Ho-Baillie, A. W. Y. Monolithic Perovskite−Perovskite−Silicon Triple-Junction Tandem Solar Cell with an Efficiency of over 20%. *ACS Energy Lett.* **2022**, *7*, 3003−3005.

(7) Choi, Y. J.; Lim, S. Y.; Park, J. H.; Ji, S. G.; Kim, J. Y. Atomic Layer Deposition-Free Monolithic Perovskite/Perovskite/Silicon Triple-Junction Solar Cells. *ACS Energy Lett.* **2023**, *8*, 3141−3146.
(8) Huang, F.; Dkhissi, Y.; Huang, W.; Xiao, M.; Benesperi, I.; Rubanov, S.; Zhu, Y.; Lin, X.; Jiang, L.; Zhou, Y.; Gray-Weale, A.; Etheridge, J.; McNeill, C. R.; Caruso, R. A.; Bach, U.; Spiccia, L.; Cheng, Y.-B. Gas-assisted preparation of lead iodide perovskite films consisting of a monolayer of single crystalline grains for high efficiency planar solar cells. *Nano Energy* **2014**, *10*, 10−18.
(9) Babayigit, A.; D'Haen, J.; Boyen, H.-G.; Conings, B. Gas Quenching for Perovskite Thin Film Deposition. *Joule* **2018**, *2*, 1205−1209.
(10) Sala, J.; Heydarian, M.; Lammar, S.; Abdulraheem, Y.; Aernouts, T.; Hadipour, A.; Poortmans, J. Compositional Investigation for Bandgap Engineering of Wide Bandgap Triple Cation Perovskite. *ACS Appl. Energy Mater.* **2021**, *4*, 6377−6384.
(11) Jiang, Q.; Tong, J.; Scheidt, R. A.; Wang, X.; Louks, A. E.; Xian, Y.; Tirawat, R.; Palmstrom, A. F.; Hautzinger, M. P.; Harvey, S. P.; Johnston, S.; Schelhas, L. T.; Larson, B. W.; Warren, E. L.; Beard, M. C.; Berry, J. J.; Yan, Y.; Zhu, K. Compositional texture engineering for highly stable wide-bandgap perovskite solar cells. *Science* **2022**, *378*, 1295−1300.
(12) Bush, K. A.; Frohna, K.; Prasanna, R.; Beal, R. E.; Leijtens, T.; Swifter, S. A.; McGehee, M. D. Compositional Engineering for Efficient Wide Band Gap Perovskites with Improved Stability to Photoinduced Phase Segregation. *ACS Energy Letters* **2018**, *3*, 428−435.
(13) Hou, T.; Zhang, M.; Yu, W.; Wang, X.; Gu, Z.; Chen, Q.; Lan, L.; Sun, X.; Huang, Y.; Zheng, B.; Liu, X.; Green, M. A.; Hao, X. Low-pressure accessible gas-quenching for absolute methylammonium-free perovskite solar cells. *J. Mater. Chem. A* **2022**, *10*, 2105−2112.
(14) Tang, S.; Bing, J.; Zheng, J.; Tang, J.; Li, Y.; Mayyas, M.; Cho, Y.; Jones, T. W.; Yang, T.C.-J.; Yuan, L.; Tebyetekerwa, M.; Nguyen, H. T.; Nielsen, M. P.; Ekins-Daukes, N. J.; Kalantar-zadeh, K.; Wilson, G. J.; McKenzie, D. R.; Huang, S.; Ho-Baillie, A. W. Complementary bulk and surface passivations for highly efficient perovskite solar cells by gas quenching. *Cell Reports Physical Science* **2021**, *2*, No. 100511.
(15) Lin, R.; Xu, J.; Wei, M.; Wang, Y.; Qin, Z.; Liu, Z.; Wu, J.; Xiao, K.; Chen, B.; Park, S.M.; Chen, G.; Atapattu, H.R.; Graham, K.R.; Xu, J.; Zhu, J.; Li, L.; Zhang, C.; Sargent, E.H.; Tan, H. All-perovskite tandem solar cells with improved grain surface passivation. *Nature* **2022**, *603*, 73.
(16) Chen, H.; Maxwell, A.; Li, C.; Teale, S.; Chen, B.; Zhu, T.; Ugur, E.; Harrison, G.; Grater, L.; Wang, J.; Wang, Z.; Zeng, L.; Park, S. M.; Chen, L.; Serles, P.; Awni, R. A.; Subedi, B.; Zheng, X.; Xiao, C.; Podraza, N. J.; Filleter, T.; Liu, C.; Yang, Y.; Luther, J. M.; de Wolf, S.; Kanatzidis, M. G.; Yan, Y.; Sargent, E. H. Regulating surface potential maximizes voltage in all-perovskite tandems. *Nature* **2023**, *613*, 676−681.
(17) Lin, R.; Wang, Y.; Lu, Q.; Tang, B.; Li, J.; Gao, H.; Gao, Y.; Li, H.; Ding, C.; Wen, J.; Wu, P.; Liu, C.; Zhao, S.; Xiao, K.; Liu, Z.; Ma, C.; Deng, Y.; Li, L.; Fan, F.; Tan, H. All-perovskite tandem solar cells with 3D/3D bilayer perovskite heterojunction. *Nature* **2023**, DOI: 10.1038/s41586-023-06278-z.
(18) Hadipour, A.; de Boer, B.; Blom, P. W. M. Organic Tandem and Multi-Junction Solar Cells. *Adv. Funct. Mater.* **2008**, *18*, 169−181.
(19) Heydarian, M.; Messmer, C.; Bett, A. J.; Heydarian, M.; Chojniak, D.; Kabaklı, Ö.Ş.; Tutsch, L.; Bivour, M.; Siefer, G.; Schubert, M. C.; Goldschmidt, J. C.; Hermle, M.; Glunz, S. W.; Schulze, P. S. C. Maximizing Current Density in Monolithic Perovskite Silicon Tandem Solar Cells. *Sol. RRL* **2023**, *7*, 2200930.
(20) Kabaklı, Ö.Ş.; Kox, J.; Tutsch, L.; Heydarian, M.; Bett, A. J.; Lange, S.; Fischer, O.; Hagendorf, C.; Bivour, M.; Hermle, M.; Schulze, P. S.; Goldschmidt, J. C. Minimizing electro-optical losses of ITO layers for monolithic perovskite silicon tandem solar cells. *Sol. Energy Mater. Sol. Cells* **2023**, *254*, No. 112246.
(21) Al-Ashouri, A.; Köhnen, E.; Li, B.; Magomedov, A.; Hempel, H.; Caprioglio, P.; Márquez, J. A.; Morales Vilches, A. B.; Kasparavicius, E.; Smith, J. A.; Phung, N.; Menzel, D.; Grischek, M.; Kegelmann, L.; Skroblin, D.; Gollwitzer, C.; Malinauskas, T.; Jošt, M.; Matič, G.; Rech, B.; Schlatmann, R.; Topič, M.; Korte, L.; Abate, A.; Stannowski, B.; Neher, D.; Stolterfoht, M.; Unold, T.; Getautis, V.; Albrecht, S. Monolithic perovskite/silicon tandem solar cell with 29% efficiency by enhanced hole extraction. *Science* **2020**, *370*, 1300−1309.
(22) Abdollahi Nejand, B.; Ritzer, D. B.; Hu, H.; Schackmar, F.; Moghadamzadeh, S.; Feeney, T.; Singh, R.; Laufer, F.; Schmager, R.; Azmi, R.; Kaiser, M.; Abzieher, T.; Gharibzadeh, S.; Ahlswede, E.; Lemmer, U.; Richards, B. S.; Paetzold, U. W. Scalable two-terminal all-perovskite tandem solar modules with a 19.1% efficiency, Nat. *Energy* **2022**, *7*, 620−630.
(23) Chen, W.; Zhu, Y.; Xiu, J.; Chen, G.; Liang, H.; Liu, S.; Xue, H.; Birgersson, E.; Ho, J. W.; Qin, X.; Lin, J.; Ma, R.; Liu, T.; He, Y.; Ng, A.M.-C.; Guo, X.; He, Z.; Yan, H.; Djurišić, A. B.; Hou, Y. Monolithic perovskite/organic tandem solar cells with 23.6% efficiency enabled by reduced voltage losses and optimized interconnecting layer, Nat. *Energy* **2022**, *7*, 229−237.
(24) Bardecker, J. A.; Ma, H.; Kim, T.; Huang, F.; Liu, M. S.; Cheng, Y.-J.; Ting, G.; Jen, A.K.-Y. Self-assembled electroactive phosphonic acids on ITO: Maximizing hole-injection in polymer light-emitting diodes. *Adv. Funct. Mater.* **2008**, *18*, 3964−3971.
(25) Thiesbrummel, J.; Peña-Camargo, F.; Brinkmann, K. O.; Gutierrez-Partida, E.; Yang, F.; Warby, J.; Albrecht, S.; Neher, D.; Riedl, T.; Snaith, H. J.; Stolterfoht, M.; Lang, F. Understanding and Minimizing VOC Losses in All-Perovskite Tandem Photovoltaics. *Adv. Energy Mater.* **2023**, *13*, 2202674.
(26) Meusel, M.; Baur, C.; Létay, G.; Bett, A. W.; Warta, W.; Fernandez, E. Spectral response measurements of monolithic GaInP/Ga(In)As/Ge triple-junction solar cells: Measurement artifacts and their explanation. *Progress in Photovoltaics: Research and Applications* **2003**, *11*, 499−514.
(27) International Electrotechnical, Photovoltaic devices − Part 8-1: Measurement of spectral responsivity of multi-junction photovoltaic (PV) devices, 1st ed., IEC: 2017.
(28) Meusel, M.; Adelhelm, R.; Dimroth, F.; Bett, A. W.; Warta, W. Spectral mismatch correction and spectrometric characterization of monolithic III-V multi-junction solar cells. *Progress in Photovoltaics: Research and Applications* **2002**, *10*, 243−255.
(29) Moriarty, T.; Jablonski, J.; Emery, K. Algorithm for building a spectrum for NREL's One-Sun Multi-Source Simulator. In *Proceedings of the 38th IEEE Photovoltaic Specialists Conference (PVSC)*, Austin, Texas, USA; IEEE: 2012; pp 1291−1295.
(30) Chojniak, D.; Bett, A.J.; J., Hohl-Ebinger; Reichmuth, S. K.; Schachtner, M.; Siefer, G. LED solar simulators − A spectral adjustment procedure for tandem solar cells. In: *SILICONPV 2022, THE 12TH INTERNATIONAL CONFERENCE ON CRYSTALLINE SILICON PHOTOVOLTAICS*, Konstanz, Germany; AIP Publishing: 2023; p 30003.
(31) Isikgor, F. H.; Maksudov, T.; Chang, X.; Adilbekova, B.; Ling, Z.; Hadmojo, W. T.; Lin, Y.; Anthopoulos, T. D. Monolithic Perovskite−Perovskite−Organic Triple-Junction Solar Cells with a Voltage Output Exceeding 3 V. *ACS Energy Lett.* **2022**, *7*, 4469−4471.
(32) Wang, Z.; Zeng, L.; Zhu, T.; Chen, H.; Chen, B.; Kubicki, D.J.; Balvanz, A.; Li, C.; Maxwell, A.; Ugur, E.; Dos Reis, R.; Cheng, M.; Yang, G.; Subedi, B.; Luo, D.; Hu, J.; Wang, J.; Teale, S.; Mahesh, S.; Wang, S.; Hu, S.; Jung, E.; Wei, M.; Park, S.M.; Grater, L.; Aydin, E.; Song, Z.; Podraza, N.J.; Lu, Z.-H.; Huang, J.; Dravid, V.P.; de Wolf, S.; Yan, Y.; Grätzel, M.; Kanatzidis, M.; Sargent, E. Suppressed phase segregation for triple-junction perovskite solar cells. *Nature* **2023**, *618*, 74.